

Energy Consumption in Wireless Systems Equipped with RES, UAVs, and IRSs

Adam Samorzewski*

**Institute of Radiocommunications, Poznan University of Technology, Poznan, Poland*

Abstract — The paper considers the characteristics of the energy budget for mobile base stations (BSs) in the form of Unmanned Aerial Vehicles (UAVs) equipped with Radio Frequency (RF) transceivers, Intelligent Reconfigurable Surfaces (IRSs), and Renewable Energy Sources (RESs). The obtained results highlight the benefits and challenges related to using the aforementioned mobile base stations from the energy side. The research cases took into account two types of UAV devices – multirotor and fixed-wing (airplane-like).**††

Keywords — 6G, power consumption, Renewable Energy Sources, Intelligent Reconfigurable Surfaces, Unmanned Aerial Vehicles, wireless systems

1. Introduction

In recent years, obtaining energy from solar radiation has become a very common solution that finds application not only in industry but also in many different areas of everyday life. The process of obtaining solar energy is carried out using generators in the form of so-called photovoltaic panels (PV – Photovoltaics). The current market attractiveness of photovoltaics results not only from the ecological approach to obtaining energy resources but also from the prices of solar modules, which have been on a downward trend for the last few years [1]. Therefore, it is not surprising that photovoltaic panels are now also used in telecommunications systems. Particular benefits can be seen from the perspective of heterogeneous wireless systems such as mobile networks.

Wind energy has also gained momentum. Generating energy from wind power is a process that depends mainly on the location, current weather conditions, and altitude above sea level. A generator that extracts energy from the wind is called a wind turbine (WT). A wind turbine converts the flowing wind speed into mechanical energy and then into

electrical energy. Wind energy can be a good alternative to solar energy, and for some locations or seasons, it may turn out to be an even more reliable solution [2], [3].

Current wireless systems are powered mainly by conventional energy sources, the utilization of which is still progressing. Due to the increasing transmission (service) requirements of Information and Communication Technology (ICT) networks, with each subsequent year, they show an increasing energy demand compared to previous years. Equipping wireless network access points with Renewable Energy Sources (RESs) could reduce or completely eliminate the demand for electricity from conventional sources. This, in turn, would not only reduce carbon dioxide (CO₂) emissions to the atmosphere but would also slow down the consumption of non-renewable resources. However, despite the benefits of RESs, they also have one basic disadvantage – the supply of energy resources is not guaranteed in an even and continuous manner due to changing weather conditions. Therefore, it may be necessary to engage more than one type of renewable source at the same time or to develop algorithms to optimize the use of available energy [2]–[4].

In addition, one of the paradigms in present and future telecommunications systems is the provision of services in hard-to-reach areas. Such areas are characterized by unfavorable conditions for the development of telecommunications infrastructure, which result, for example, from the terrain or the inability to connect to the existing telecommunications and energy networks. In a situation where the first problem could be solved by using mobile access nodes (e.g., drones) and involving wireless connectivity for backhaul communication, the second case is extremely difficult to cope with [5]. However, considering the off-grid approach in the context of powering individual system components, RES generators (e.g., photovoltaic panels, wind turbines) in combination with an autonomous battery system could be able to meet the energy needs of the Radio Access Network (RAN) [6]. However, this requires appropriate modeling of the energy cycle of the system, i.e., predicting the results of production and the use of energy resources in time in such a way as to ensure their adequate amount for each type of load on network links [7].

In the context of increasing the efficiency of wireless systems, the Intelligent Reflective Surface (IRS) is proving to be a very promising concept. The IRS is a device in the form of a flat surface containing a large number of passive reflecting elements. Each of these elements is able to independently cause a controlled change in the amplitude

**The work has been realized within research project no. 2021/43/B/ST7/01365 funded by the National Science Center in Poland.

††Copyright © 2023 National Institute of Telecommunications in Poland. Personal use is permitted. For any other purposes, permission must be obtained from the National Institute of Telecommunications in Poland by emailing journal@jit.pl. This is the author's version of an article that has been published in the *Journal of Telecommunications and Information Technology (JTIT)* by the National Institute of Telecommunications in Poland. Changes were made to this version by the publisher before publication, the final version of the record is available at: <https://dx.doi.org/10.26636/jtit.2023.170923>. To cite the paper use: A. Samorzewski, "Energy Consumption in Wireless Systems Equipped with RES, UAVs, and IRSs," *Journal of Telecommunications and Information Technology (JTIT)*, 2023, no. 2, pp. 35–40, doi: 10.26636/jtit.2023.170923 or visit <https://jit.pl/jtit/article/view/1175/1161>.

and/or phase of the incident radio signal. The dense distribution of IRS surfaces in the wireless network and intelligent coordination of their reflections can make the propagation of the radio signal (wireless channels) between transmitters and receivers flexibly reconfigurable. This, in turn, can solve the problems of wireless channel dropout and interference. In addition, thanks to the use of IRS, improvements in the throughput and reliability of wireless communication can be achieved [8].

This paper proposes models of energy consumption for wireless access networks whose nodes are Unmanned Aerial Vehicles (UAVs) equipped with Intelligent Reconfigurable Surfaces (IRSs) and powered by Renewable Energy Sources (RESs). In the contribution, the characteristics of the energy balance for the aforementioned system depending on the type of equipment and weather conditions have been also investigated.

The paper has been organized as follows: first, the mathematical models for energy consumption and harvesting have been described; next, the simulation setup configuration has been presented. After the third section, the results of performed simulation runs have been overviewed. Finally, the last part is focused on conclusions summarizing the contribution of the paper.

2. Energy Models

In order to estimate the energy efficiency of the considered wireless system, an extremely important step is to precisely configure the study scenario and to model the energy cycle for the components of the network. The simulation scenario considered in the paper assumes the use of a UAV device as a base station (BS), which is equipped with photovoltaic panels and wind turbines for energy generation. In addition, the mobile access node has one IRS device to extend the range of the emitted radio signal and improve the performance of the wireless system. The used UAV base station may be of the multirotor or fixed-wing type, which will allow comparing the energy balance characteristics for both kinds. The UAV node is able to maintain a connection with the major station on the backhaul link implemented in accordance with microwave (MW) technology and on the access link realized in the Radio Frequency (RF) band. The UAV base station hovers/flyes above the ground in free space in the city of Poznan. Where a multirotor mobile station can maintain a fixed position in the sky, a fixed-wing type station is forced to follow some flight trajectory. The work considers a static case in which drones do not change their position (multirotor) or trajectory (fixed-wing) – optimization of the location of the UAV station and its impact on the functioning of the network is the subject of parallel activities. However, the paper takes into account the impact of atmospheric factors such as wind or cloud cover on both the consumption of energy resources and their harvesting from RESs. The power consumption (PC) characteristics take into account the utilization related to the hovering/flying of the UAV station and the provision of services by it in the considered

area using the MIMO technique and IRS device. However, in the context of obtaining energy resources from RESs, the generation processes were analyzed both for different times of the day and year, as well as for different wind speeds, solar radiation densities, and types of cloud cover, i.e., different cloud thicknesses. Telecommunications traffic in the network is assumed to be fixed.

2.1. Energy Consumption

The power consumption for a fixed-wing UAV mobile base station ($P_{UAV,FW}$) in time step t can be described by the following formula [9]:

$$P_{UAV,FW}(t) = \left| c_1 v_{UAV}^3(t) + \frac{c_2}{v_{UAV}(t)} \left(1 + \frac{a_{\perp}^2(t)}{g^2} \right) + m_{ALL} a_{\parallel}(t) v_{UAV}(t) \right|, \quad (1)$$

where v_{UAV} is the forward flight velocity of the UAV, a_{\perp} and a_{\parallel} are the centripetal acceleration when the base station moves along the circular trajectory, and the forward acceleration, respectively. The m_{ALL} is the sum of the masses of all the components of a particular UAV, i.e., the weights of the UAV itself (m_{UAV}), its battery system (m_{BATT}), RES generators (m_{PV} , m_{WT}), and additional equipment (m_{RF} , m_{IRS} , m_{PKG}). Next, the g parameter is the gravitational acceleration, and c_1 and c_2 are the parameters described by the following formulas [9]:

$$c_1 \triangleq \frac{1}{2} \rho C_{D_0} S, \quad c_2 \triangleq \frac{2W^2}{\pi e_0 A_R \rho S}, \quad (2)$$

where ρ is the air density (calculated according to the formula from [10]), C_{D_0} is the zero-lift drag coefficient and S is the reference area. The parameter of $W = m_{ALL} \cdot g$ is the weight force of the UAV device. Whereas e_0 and A_R are wingspan efficiency (Oswald efficiency) and UAV wing aspect ratio, respectively.

As for the power consumption of multirotor base stations ($P_{UAV,MR}$) in the current time step t , its mathematical model is as follows [11]:

$$P_{UAV,MR}(t) = \frac{d_0}{2} \rho n s A_{UAV} v_{UAV}^3(t) + P_0(t) \left(1 + \frac{3v_{UAV}^2(t)}{\Omega^2(t) R^2} \right) + P_1 \tilde{\kappa}(t) \left(\sqrt{\tilde{\kappa}(t) + \frac{v_{UAV}^4(t)}{4v_0^4}} - \frac{v_{UAV}^2(t)}{2v_0^2} \right)^{\frac{1}{2}}, \quad (3)$$

where Ω , R , v_0 are the angular velocity, radius and mean induced velocity in the hover of a single rotor of a UAV, respectively. The latter can be expressed as $v_0 = \sqrt{\frac{W}{2\rho A_{UAV}}}$, where A_{UAV} is the area of a rotor of the UAV. The parameters of n and s are the number of UAV rotors and the solidity of a single one. In turn, $\tilde{\kappa}$ and d_0 are the ratio of thrust to weight forces of the UAV and the fuselage drag ratio. The values of the parameters of P_0 (in time step t) and P_1 are described by

the following formulas [11]:

$$P_0(t) = \frac{\delta}{8} \rho n s A_{\text{UAV}} \Omega^3(t) R^3, \quad P_i = (1+k) \left(\frac{W^3}{2\rho n A_{\text{UAV}}} \right), \quad (4)$$

where δ is the profile drag coefficient and k is the incremental correction factor to induced power.

The power utilized by the IRS device connected to the UAV (P_{IRS}) and RF transceiver (P_{MIMO}) has been evaluated in accordance with the mathematical models contained in [12] and [13], respectively. Those models are described by the equations (5) and (6) attached below:

$$P_{\text{IRS}}(t, b) = N(t) \cdot P_n(b), \quad (5)$$

$$\begin{aligned} P_{\text{MIMO}}(t) = & P_{\text{FIX}} + P_{\text{TC}}(M(t)) + P_{\text{CE}}(M(t), K(t)) \quad (6) \\ & + P_{\text{C/D}}(\text{TR}_{\text{UL}}(t), \text{TR}_{\text{DL}}(t)) + P_{\text{BH}}(\text{TR}_{\text{UL}}(t), \text{TR}_{\text{DL}}(t)) \\ & + P_{\text{SP}}(M(t), K(t)) + \frac{P_{\text{TX}}(t)}{\mu_{\text{PA}}}, \end{aligned}$$

where P_{FIX} is the fixed power demand of a particular mobile base station, P_{TC} is the consumption of transceiver chains, and P_{CE} , $P_{\text{C/D}}$, and P_{SP} are the power components utilized for operations performed within a base station such as channel estimation, data coding/decoding, and signal processing. Next, P_{BH} and P_{TX} are the powers related to mobile data flow, i.e., load-dependent MW backhaul and RF fronthaul, respectively. The parameters of $M(t)$ and $K(t)$ are the numbers of active antenna elements and served users in the current time step t . Next, μ_{PA} is the efficiency of the power amplifier. Finally, the TR_{UL} and TR_{DL} components are uplink (UL) and downlink (DL) total data throughputs, which can change over time. In addition, for channel estimation and signal processing the use of the minimum mean-squared error (MMSE) scheme has been assumed.

Eq. (5) consists of only two parameters – N and P_n , which are the number of identical reflecting elements that effectively perform phase shifting on the impinging signal, and the power consumption of each phase shifter. The value of the second one is dependent on the bit resolution b of the used phase shifter.

2.2. Energy Generation

Models of harvesting energy resources by the applied generators of Renewable Energy Sources are presented below. The power generated by the photovoltaic panel of the UAV base station (P_{PV}) can be described by the following mathematical formula [14]:

$$P_{\text{PV}}(t) = P_{\text{r,PV}} f_{\text{PV}} \left(\frac{\overline{G}_{\text{T}}(t)}{\overline{G}_{\text{T,STC}}} \right) [1 + \alpha_{\text{P}} (T_{\text{c}}(t) - T_{\text{c,STC}})], \quad (7)$$

where $P_{\text{r,PV}}$ is the rated capacity of the PV array (its output power under Standard Test Conditions – STC), f_{PV} is the PV derating factor, and α_{P} is the temperature coefficient of

power, which indicates how strongly the PV array power output depends on the cell temperature. In turn, \overline{G}_{T} and $\overline{G}_{\text{T,STC}}$ are the solar incident radiation on the PV array in the current time step t and at STC, respectively. Whereas T_{c} and $T_{\text{c,STC}}$ are also the PV cell temperature in the current time step t and under STC, respectively. The PV cell temperature can be calculated with the equation contained in [14].

The power generated by the wind turbine (P_{WT}) can be described as follows [15]:

$$P_{\text{WT}}(t) = \begin{cases} 0, & \text{if } v_{\text{w}}(t) < v_{\text{in}} \\ F(v_{\text{w}}(t)), & \text{if } v_{\text{in}} \leq v_{\text{w}}(t) < v_{\text{r}} \\ P_{\text{r,WT}}, & \text{if } v_{\text{r}} \leq v_{\text{w}}(t) \leq v_{\text{out}}, \end{cases} \quad (8)$$

where v_{in} , v_{out} , v_{w} are the cut-in and cut-out speed of the wind turbine (defining the range of wind speed values for which the wind turbine is able to generate energy resources), and the instantaneous wind speed, respectively. Next, F is the power curve function of the WT, which determines its energy harvesting characteristic. Finally, P_{r} and v_{r} denote the rated output power of the used wind turbine and minimum wind speed ($v_{\text{in}} < v_{\text{r}} < v_{\text{out}}$), for which this power can be achieved. The power curve function normalized in the relation to the maximum value of the WT's output power has been presented in Fig. 2.2.. The corrections of wind speed (to get its correct value at the altitude of the generator) and WT output power (which depends on the current air density) were realized in accordance with [14].

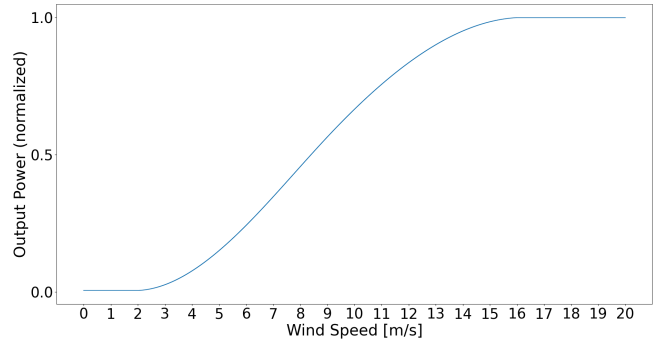


Fig. 1

Power curve function of wind turbine (based on [16]).

3. Simulation Setup

The examined base stations were UAVs of the multirotor and fixed-wing type. Furthermore, each UAV BS was also equipped with a single RF transceiver and IRS device. The impact of RES generators enabling on the overall power consumption of the mobile base station has been also taken into consideration. Thus, four study cases have been simulated. The first investigates PC in different seasons of the year, which is caused by the UAV and its additional equipment (IRS device and RF transceiver) with no RES generators on board. The second, third, and fourth cases take

into account as well the power consumption resulting from powering the mobile BS with a PV, WT, and both of them, respectively. The examination of energy generation from RESs has been considered based on the real products, the specifications of which can be found in [16] and [17].

Simulations have been prepared using the Python programming language. As the outcomes, the characteristics for energy consumption of the mobile base stations as well as for energy harvesting of the RES generators have been evaluated. The results have been prepared for four different dates starting various seasons of the last year – vernal equinox (20th March 2022), summer solstice (21st June 2022), autumn equinox (23rd September 2022), and winter solstice (21st December 2022). All the weather data used in the simulations are the real historical data taken from the following source [18] for the city of Poznan (Poland). The one exception is the global solar radiation density which was estimated by using the MAC model [19].

All the prepared energy characteristics charts have been normalized in relation to the maximum values obtained for them. Furthermore, in Tab. 3. the values for the parameters of the mathematical energy models aforementioned in Section 2. have been highlighted. The values of the parameters related to the power consumption model for RF transmission (not contained in Tab. 3.) were taken from Tab. 5.3 in [13].

4. Results

Below are the charts with the characteristics of energy consumption by the mobile base stations as well as of energy generation by their RES generators have been shown. A particular color of the plots and bars is strictly associated with a specific season of the year: blue – the vernal equinox, yellow – the summer solstice, green – the autumn equinox, and red – the winter solstice.

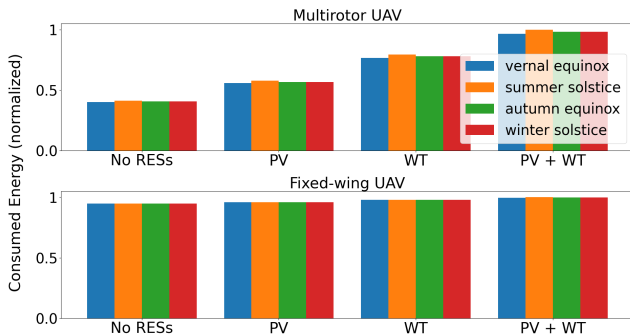


Fig. 2

Energy consumption character. for multirotor and fixed-wing UAVs.

In Fig. 4., the normalized energy utilization process for the different UAV types has been presented. The chart at the top denotes the characteristics of the multirotor UAV, and the second one placed below describes the consumed energy by the fixed-wing type. The values presented in the figure

Table 1
VALUES OF THE SIMULATION PARAMETERS
[7], [9], [11], [12], [16], [17], [20]–[23]

Symbol	Quantity	Value	Unit
m_{UAV}	mass of a UAV	5.0	[kg]
m_{BATT}	mass of a battery	0.94	[kg]
m_{RF}	mass of a RF trans.	2.0	[kg]
m_{IRS}	mass of an IRS dev.	1.0	[kg]
m_{PV}	mass of a PV panel	2.78	[kg]
m_{WT}	mass of a WT	6.0	[kg]
m_{PKG}	mass of an addi. package	0.0	[kg]
Ω	rotor angular velocity	300.0*	[rad/s]
v_{UAV}	velocity of a UAV	0.0*	[m/s]
v_{in}	cut-in speed of a WT	10.0**	[m/s]
v_{out}	cut-out speed of a WT	2.0	[m/s]
v_r	rated speed of a WT	20.0	[m/s]
a_{\parallel}	UAV's forward accel.	16.0	[m/s]
a_{\perp}	UAV's centripetal accel.	0.0**	[m/s ²]
g	gravitational accel.	0.0**	[m/s ²]
δ	profile drag coefficient	9.81	[m/s ²]
k	incre. correction factor	0.012*	
$\tilde{\kappa}$	thrust-to-weight ratio	0.1*	
d_0	fuselage drag ratio	1*	
C_{D_0}	zero-lift drag coeffi.	14.52*	
e_0	Oswald efficiency	0.01**	
A_R	UAV's wing aspect ratio	0.85**	
S	UAV's ref. (wing) area	118.81**	[m ²]
A_{UAV}	UAV's rotor area	1.0**	[m ²]
R	UAV's rotor radius	0.071*	[m]
s	UAV's rotor solidity	0.15*	
n	number of rotors	0.067*	
M	number of antenna ele.	8*	
K	number of users	16	
N	number of reflect. ele.	10	
b	phase shifter resolution	16	[bit]
TR_{UL}	UL data throughput	6	[Mbps]
TR_{DL}	DL data throughput	50.0	[Mbps]
f_{PV}	PV's derating factor	100.0	
α_p	tem. coeffi. of power	0.72	[%/°C]
$T_{c,\text{STC}}$	STC solar cell temper.	-0.5	[°C]
$G_{t,\text{STC}}$	STC solar incident radi.	25	[W]
$P_{r,\text{PV}}$	PV panel's rated power	1000	[W]
$P_{r,\text{WT}}$	rated power of a WT	20.0	[W]
P_n	power of a phase shifter	30.0	[W]
P_{TX}	transmit power of a UAV	7.8	[W]
μ_{PA}	power amplifier efficiency	15.0	[W]

* only for the multirotor type

** only for the fixed-wing type

were not normalized in the relation to the same value, but each one was scaled according to the maximum value obtained for a particular study case. Thus, lower consumption that can be observed for the multirotor does not mean this type of UAV uses less energy than the fixed-wing type. The main goal of the investigation was to highlight the impact of adding extra equipment to the UAV weight on the energy utilization itself in different seasons of the year. For a hovering multirotor UAV the amount of its total mass has a crucial

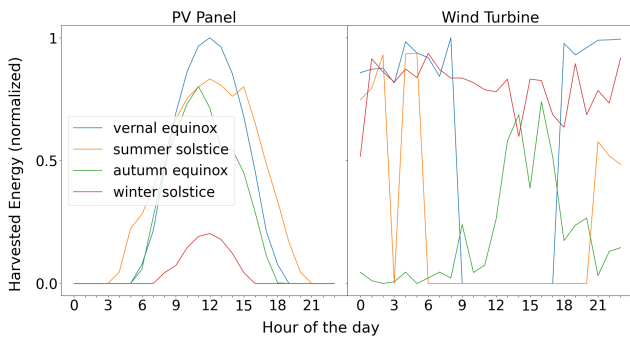


Fig. 3

Energy generation characteristics for PV panel and wind turbine.

meaning to its energy demand. By adding a PV panel and wind turbine (around 9 kg) to the base station, its energy consumption increases almost twice. For different seasons, some deviations in the use of energy resources by the multirotor UAV can be observed as well. The reason for that is fluctuating air density value during the year. For the UAV of the fixed-wing type, aforementioned weight and weather dependencies can be noticed as well, but their impact on PC is not so significant as for the multirotor BS. On the other hand, within this paper, only one situation was considered, in which the fixed-wing UAV is flying with a constant velocity equal to 10 m/s. The real impact might be seen by studying changes in energy utilization of the drone lifting various weight loads from the ground, or studying changes in its aerodynamic characteristics. Both cases will be considered in future work.

Fig. 4. presents the energy harvesting processes of the PV panel and wind turbine used in the contribution to power the UAV BSs. The characteristics have been prepared based on the real equipment products, the specifications of which can be found in [16] and [17]. The charts contained in Fig. 4. highlight the energy gain that can be achieved for different seasons of the year. Based on that it is possible to assess when equipping the mobile base station with a particular RES generator is beneficial. For instance, in the summer season, the PV panel is the most effective and WT the least. In the wintertime of the year, the situation is the opposite. Interestingly, the peak of energy harvesting for both generators can be observed for the vernal equinox although it is not the most effective season for producing power by PV panels or wind turbines. However, the reason for that is the limitations of RES generators, i.e., each type has its temperature or wind speed ranges, in which they can produce renewable energy resources. In addition, the output power of the PV panel is greatly influenced by the current temperature of its solar cells (dependent, e.g., on the current ambient temperature) and the opacity of the clouds in the sky. Thus, an increase in air temperature and the amount of clouds can cause a decrease in energy harvesting efficiency.

5. Conclusions

In this paper, the characteristics of energy utilization and generation by the two types of UAV mobile base stations equipped with RF transceivers, IRS devices, and RES generators (PV panels and wind turbines) have been investigated. Obtained results highlight the impact of the UAV's equipment on the energy balance for different seasons of the year. The paper's outcomes seem to be valuable for the process of network planning for future wireless systems considering the use of UAVs, IRSs, and RESs.

References

- [1] V. Kozlov and W. Salabun, „Challenges in Reliable Solar Panel Selection Using MCDA Methods”, Elsevier, *Procedia Computer Science*, vol. 192, pp. 4913–23, 2021.
- [2] A. Jahid, M. K. H. Monju, M. E. Hossain, and M. F. Hossain, „Renewable Energy Assisted Cost Aware Sustainable Off-Grid Base Stations with Energy Cooperation”, *IEEE Access*, vol. 6, pp. 60900–20, 2018.
- [3] M. Deruyck, S. Bova, G. Vallero, M. Meo, L. Martens, and W. Joseph, „Designing a Hybrid Renewable Energy Source System to Feed the Wireless Access Network”, *Sustainable Energy, Grids and Networks*, vol. 31, 2022.
- [4] A. Samorzewski and A. Kliks, „User Allocation in Heterogeneous Network Supplied by Renewable Energy Sources”, *2021 17th International Conference on Wireless and Mobile Computing, Networking and Communications (WiMob), 11-13.10.2021, Bologna, Italy*, pp. 419–22, 2021.
- [5] A. Chaoub, M. Giordani, B. Lall, V. Bhatia, A. Kliks, et al., „6G for Bridging the Digital Divide: Wireless Connectivity to Remote Areas”, *IEEE Wireless Communications*, vol. 29, no. 1, pp. 160–8, 2022.
- [6] M. S. Hossain, A. Jahid, K. Z. Islam, M. H. Alsharif, et al., „Towards Energy Efficient Load Balancing for Sustainable Green Wireless Networks under Optimal Power Supply”, *IEEE Access*, vol. 8, pp. 200635–54, 2020.
- [7] O. Arnold, F. Richter, G. P. Fettweis, and O. Blume, „Power Consumption Modeling of Different Base Station Types in Heterogeneous Cellular Networks”, *IEEE, Future Network & Mobile Summit*, 2010.
- [8] Q. Wu, S. Zhang, B. Zheng, C. You, and R. Zhang, „Intelligent Reflecting Surface-Aided Wireless Communications: A Tutorial”, *IEEE Transactions on Communications*, vol. 69, no. 5, pp. 3313–51, 2021.
- [9] Y. Zeng and R. Zhang, „Energy-Efficient UAV Communication With Trajectory Optimization”, *IEEE Transactions on Wireless Communications*, vol. 16, no. 6, pp. 3747–60, 2017.
- [10] D. Czernia and B. Szyk, „Air Density Calculator”, Available at: <https://www.omnicalculator.com/physics/air-density>, Accessed: 21 March 2023.
- [11] Y. Zeng, J. Xu, and R. Zhang, „Energy Minimization for Wireless Communication With Rotary-Wing UAV”, *IEEE Transactions on Wireless Communications*, vol. 18, no. 4, pp. 2329–45, 2019.
- [12] C. Huang, A. Zappone, G. C. Alexandropoulos, M. Debbah, and C. Yuen, „Reconfigurable Intelligent Surfaces for Energy Efficiency in Wireless Communication”, *IEEE Transactions on Wireless Communications*, vol. 18, no. 8, pp. 4157–70, 2019.
- [13] E. Björnson, J. Hoydis, and L. Sanguinetti, „Massive MIMO Networks: Spectral, Energy, and Hardware Efficiency”, *Foundations and Trends® in Signal Processing*, vol. 11, no. 3-4, pp. 154–655, 2017.
- [14] HOMER Pro v3.15, „Documentation – HOMER's Calculations”, Available at: https://www.homerenergy.com/products/pro/docs/3.15/homers_calculations.html, Accessed: 21 March 2023.
- [15] C. Carrillo, A. F. Obando Montaña, J. Cidrás, and E. Díaz-Dorado, „Review of power curve modelling for wind turbines”, *Renewable and Sustainable Energy Reviews*, vol. 21, pp. 572–81, 2013.

- [16] Saiam, „Saiam VAWT SAV-30W Specifications”, Available at: <http://www.yashikaenergy.com/pdf/sai3.pdf>, Accessed: 21 March 2023.
- [17] Solarland, „Solarland SLP020-12U Specifications & Warranty”, Available at: <https://www.solar-electric.com/lib/wind-sun/SLP020-12U.pdf>, Accessed: 21 March 2023.
- [18] Visual Crossing, „Historical Weather Data & Weather Forecast Data”, Available at: <https://www.visualcrossing.com/weather-data>, Accessed: 21 March 2023.
- [19] J. A. Davies and D. C. McKay, „Estimating solar irradiance and components”, *Solar Energy*, vol. 29, no. 1, pp. 55–64, 1982.
- [20] E. A. Franklin, „Calculations for a Grid-Connected Solar Energy System”, Available at: <https://extension.arizona.edu/sites/extension.arizona.edu/files/pubs/az1782-2019.pdf>, Accessed: 21 March 2023.
- [21] Green Cell, „Green Cell Accumulator LiFePO4 12V 12.8V 7Ah – Product card CAV09”, Available at: https://greencell.global/en/index.php?controller=attachment&id_attachment=316, Accessed: 21 March 2023.
- [22] HOMER Pro v3.15, „Documentation – Glossary”, Available at: <https://www.homerenergy.com/products/pro/docs/3.15/glossary.html>, Accessed: 21 March 2023.
- [23] F. Götten, D. F. Finger, M. Havermann, et al., „Full configuration drag estimation of short-to-medium range fixed-wing UAVs and its impact on initial sizing optimization”, *CEAS Aeronautical Journal*, vol. 12, pp. 589–603, 2021.